TABLE 1: COMPARISON BETWEEN PAST, PRESENT, AND FUTURE ORBITAL IMAGING RADAR SYSTEMS

	SEA-SAT	SIR-A	SIR-B	ALMAZ -1	ERS-1	JERS-1	SIR-C	X-SAR	ERS-2	RADAR-SAT	PRIR-ODA	ENVI-SAT	SRTM	PAL-SAR	Light-SAR
Band	L	L	L	S	C	L	C,L	X	C	C	S,L	C	C	L	L
Polarization	HH	HH	HH	HH	VV	HH	All	VV	VV	HH	HH	All	HH	HH or VV HV or VH	All
Incident Angle (°)	23	45	20-60	30-60	24	35	17-60	17-60	24	17-50	35	20-45	20-60	20-55	20
Resolution (meter)	25	30	30	15	25	18	25	25	25	10-100	30	30	30	10-100	25-100
Swath Width (km)	100	50	50	20-45	100	76	15-100	15-40	100	50-170	120	50-400	60	70-250	50-500
Orbital Platform	Satellite	Space Shuttle	Space Shuttle	Satellite	Satellite	Satellite	Space Shuttle	Space Shuttle	Satellite	Satellite	Space Station	Satellite	Space Shuttle	Satellite	Satellite
Organization	NASA	NASA	NASA	RSA (PKA)	ESA	NSDA/ MITI	NASA	DLR/ ASI	ESA	CSA	RSA/ DLR	ESA	NIMA/ NASA/ DLR/ ASI	NASDA/ MITI	NASA
Altitude (km)	790	225	225	300	790	568	225	225	785	790	394	800	233	700	790
Orbit Inclination (°)	108	57	57	72.7	97.7	97.7	57	57	97.7	98.6	51.6	100	57	98	97.7
Launch Date	1978	1981	1984	1991	1991	1992	1994	1994	1995	1995	1995	1998	2000	2002	2003
Life Time	105 days	11 days	11 days	2.5 y	3 y	2 y	11 days	11 days	3 y	5 y	2 y	5 y	11 days	3-5 y	3-5 y

Wavelengths are 3 cm for X band, 6 cm for C Band, 10 cm for S Band, and 24 cm for L Band. Polarizations are abbreviated as HH = Horizontally Transmitted and Horizontally Received, HV = Horizontally Transmitted and Vertically Received, VV = Vertically Transmitted and Vertically Received, and VH = Vertically Transmitted and Horizontally Received. Organization abbreviations are NASA = U.S. National Aeronautics and Space Administration, RSA (PKA) = Russian Space Agency, ESA = European Space Agency, NASDA = National Space Development Agency of Japan, MITI = Ministry of International Trade and Industry of Japan, DLR = Deutsches Zentrum Für Luft- und Raumfahrt or German Aerospace Center, ASI = Agenzia Spaziale Italiana or Italian Space Agency, and NIMA = U.S. National Imaging and Mapping Agency.

1992 the National Space Development Agency (NASDA) of Japan launched the Japanese Earth Resources Satellite (JERS)-1 (Moon *et al.*, 1994) (Table 1).

In 1994 NASA twice launched the Shuttle Endeavour to collect the first multi-spectral and multi-polarization SIR-C/X-SAR data between latitudes 57°N and 57°S. These data were collected with multi-look angles and swaths ranging in width between 15 and 100 km for the L and C bands and 15 and 40 km for the X band (Table 1). SIR-C/X-SAR data are advanced compared to SIR-A and SIR-B and other orbital radar data in that they were simultaneously collected at three wavelengths and multiple polarizations (Table 1). L and C bands were collected with like-polarization HH (horizontally transmitted and horizontally received) and VV (vertically transmitted and vertically received), and cross-polarization HV(horizontally transmitted and vertically received) and VH (vertically transmitted and horizontally received). X band was collected with VV only (Table 1).

The Canadian Space Agency (CSA) in 1995 put into orbit the first commercial imaging radar satellite RADARSAT (Parashar *et al.*, 1993) (Table 1). The PKA attached to MIR in the same year the first space station-borne radar system enclosed in the module PRIRODA of the German Aerospace Center (DLR = DAS).

NASA launched the Shuttle Radar Topography Mission (SRTM) in early 2000 (Farr and Kobrick, 1998; Okonek, 1999) (Table 1) to collect single-path, but repeated-take, data for interferometric uses between latitudes 60°N and 54°S. NASA also plans to utilize radar interferometry in measuring large-scale surface changes. For this purpose, the Lightweight Synthetic Aperture Radar (LightSAR) satellite mission is planned for the year 2003 (Schoonmaker, 1997; Evans and Moghaddam, 1998) (Table 1). Other future plans for orbital imaging radar include ESA ENVISAT1 (European Space Agency, 1998) (Table 1) and NASDA of Japan PALSAR satellite (NASDA, 1999).

Imaging with Orbital Radar

Orbital imaging radar systems depend on measuring the amplitude, time delay, and phase shifts of returned radar signals. Radar signals are produced by a source antenna with a side-looking geometry and measured by a receiving antenna after backscattering or volume-scattering off a surface (Zebker and Goldstein, 1986). The amplitude of the returned radar signal depends on system-related (wavelength, polarization, and incidence angle) and environment-related (surface and sub-surface roughness, slope, and dielectric properties) factors (Lewis *et al.*, 1998). These factors control three types of interaction between radar signals and the imaged surface (Lewis *et al.*, 1998): (1) reflection, (2) back-scattering, and (3) volume-scattering (Figure 1A).

Reflection

Reflection occurs when a radar signal encounters a smooth flat surface. The signal reflects away from the receiving antenna with an angle equals to that of the incident angle (Figure 1A). In this case no returning radar signal will be detected in the receiving antenna; hence smooth, flat surfaces appear dark on radar images.

Backscattering

Backscattering occurs when the radar signal encounters a rough surface. The radar waves scatter in different directions and some return to the receiving antenna (Figure 1A). Backscattering depends on the roughness level relative to the radar band wavelength. Shorter wavelengths increase the perceived surface roughness (Campbell and Campbell, 1992). Generally, a surface is considered rough if the weathering cell (roughness characteristics) equals or is greater than 10 percent of the radar band wavelength (Lewis *et al.*, 1998). In addition, at a constant wavelength, a flat surface is perceived as smoother as the look angle increases (Ford *et al.*, 1989).

Volume-Scattering

The term volume-scattering is used here to describe a returned radar signal that follows a path with more than one direction (Figure 1B). The two types of volume scattering are double-bounce and penetration (Figure 1A). Double-bounce is discussed together with normal-reflection (when the incident angle equals 90°, the path of the returning signal coincides with that of the incoming signal but is in the opposite direction) and edge-effect because they are all associated (Figure 1B).

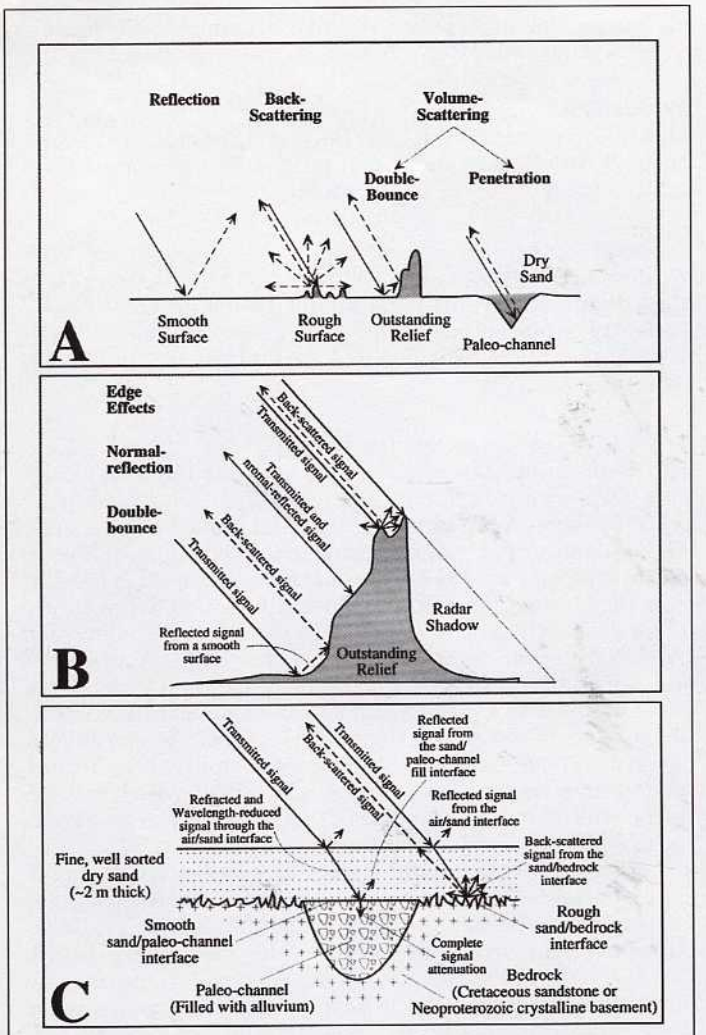

Figure 1. (A) Radar scattering mechanisms. (B) Radar double-bounce, normal-reflection, and edge-effect. (C) Radar penetration of dry sand and imaging of sub-surface paleochannels in the eastern Sahara (modified after Sabins (1997)).

Double-Bounce, Normal-Reflection, and Edge-Effect

Double-bounce occurs when the radar signal reflects from a smooth flat surface, encounters outstanding relief, and is reflected back again to the receiving antenna (Figure 1B). Outstanding relief with a surface tilted nearly perpendicular to the radar signal results in normal-reflection (Figure 1B). Outstanding objects can also cause preferential backscattering from their edges and corners (Figure 1B). This is referred to as edge-effect and corner reflectors (Ford *et al.*, 1989). Double-bounce, normal-reflection, and edge-effect result in radar illumination/shadow where bright stripes are in juxtaposition with dark stripes.

Penetration

One of the most important characteristics of radar in geologic studies of the eastern Sahara is its ability to penetrate dry sand and image the shallow sub-surface features (Roth and Elachi, 1975; McCauley *et al.*, 1982; McCauley *et al.*, 1986; Elachi *et al.*, 1984; Blom *et al.*, 1984; Schaber *et al.*, 1997; Sabins, 1997; Lewis *et al.*, 1998) (Figure 1C). The optimum conditions for sub-surface imaging with orbital radar in arid regions are (1) smooth surface of fine-grained and well-sorted sand (Roth and Elachi, 1975) (Figure 1C); (2) very dry conditions (less than 1 percent moisture content) to minimize electrical conductivity and facilitate greater radar signal penetration (Campbell and Ulrichas, 1969; Hoekstra and Delaney, 1974); (3) limited depth of sand cover (Figure 1C); experiments show that a radar signal is attenuated to 37 percent at the air/sand interface and completely attenuated at depth of more than 2 meters at 1 percent moisture content (Elachi and Granger, 1982); (4) sub-surface imaging occurs when a rough sand/bedrock interface produces strong backscattering (Elachi *et al.*, 1984) (Figure 1C); and (5) in addition to the above environment-related factors, system-related factors important in optimizing radar penetration are (a) longer wavelengths result in deeper radar penetration (Schaber *et al.*, 1997) (Figures 2A, 2B, and 2C); (b) cross-polarization enhances radar penetration (Schaber *et al.*, 1997); and (c) sub-surface features are more likely to be revealed at radar look angles greater than 30° (Elachi *et al.*, 1984).

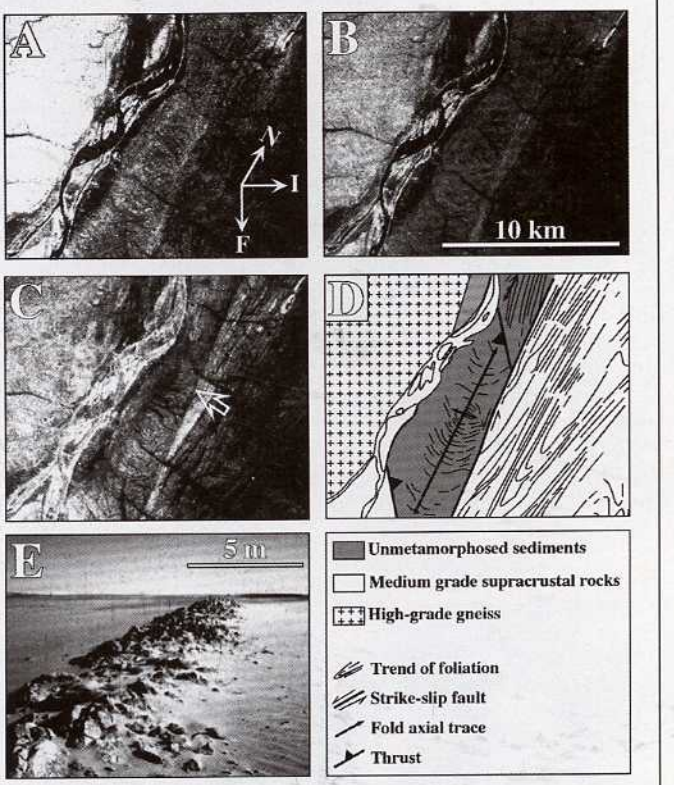

Figure 2. Images of part of the Neoproterozoic Keraf suture in northern Sudan. For location, see Plate 1. (A) X-VV image. (B) C-HH image. (C) L-HH image. (D) Lithologic and structural interpretation of the L-HH image. (E) A field photograph of a ~5 m wide ridge defining a mylonite zone associated with a sinistral shear zone in the Neoproterozoic Keraf suture. (B), (C), and (D) indicate greater depth of penetration with increasing wavelength. The L-HH image in 2C shows the shear zones because of the edge-effect caused by the narrow ridge in 2E shown by an open white arrow in 2C. This allows radar to image the ridge although it is smaller than its 30-m spatial resolution. The abbreviations in the arrows indicate north (N), radar illumination direction (I), and shuttle flight direction (F).